Journal of Molecular Structure 1271 (2023) 134046

Contents lists available at ScienceDirect

Journal of Molecular Structure

journal homepage: www.elsevier.com/locate/molstr

Tetrahydroxyphthalocyanine as a potential nonlinear optical material

Sebile Işık Büyükekşi[a], Efe Baturhan Orman[b], Ahmet Karatay[c], Nursel Açar Selçuki[d], Ali Rıza Özkaya[b], Ayhan Elmali[c], Bekir Salih[e], Abdurrahman Şengül[a,*]

[a] Department of Chemistry, Faculty of Arts and Sciences, Bülent Ecevit University, TR-67100 Zonguldak, Turkey
[b] Department of Chemistry, Marmara University, TR-34722 Göztepe, Istanbul, Turkey
[c] Department of Engineering Physics, Faculty of Engineering, Ankara University, TR-06100 Ankara, Turkey
[d] Department of Chemistry, Faculty of Science, Ege University, TR-35100 Bornova, Izmir, Turkey
[e] Department of Chemistry, Faculty of Science, Hacettepe University, TR-06800 Ankara, Turkey

ARTICLE INFO

Article history:
Received 11 June 2022
Revised 22 August 2022
Accepted 29 August 2022
Available online 30 August 2022

Keywords:
Zinc
Phthalocyanine
DFT
Nonlinear
Electrochemistry

ABSTRACT

We have synthesized a new zinc(II)-phthalocyanine (ZnPc) incorporating hydroxyl groups at the peripheral positions. This new zinc(II)-tetra-hydroxyphthalocyanine (**1**) has been characterized by high-resolution MALDI TOF MS, UV-Vis, FT-IR (ATR), and ^{1}H- and ^{13}C-NMR techniques, and further by the electrochemical measurements. DFT and TD-DFT computations were performed to model plausible structure and also analyze the electronic structure and optical properties of **1**. The effects of the polarity and hydrogen bonding ability of the hydroxyl substituents on the peripheral positions of **1** on the optical and electrochemical properties are reported in this study. The redox behavior of **1** in dimethyl sulfoxide (DMSO) was determined by voltammetry and colorimetry supported *in situ* spectroelectrochemistry. The nonlinear absorption and optical limiting (OL) properties of **1** were measured in tetrahydrofuran (THF) by utilizing the open aperture Z-scan technique with nanosecond pulses at 532 nm. The sample demonstrated good reverse saturable absorption and OL behaviors. The ultrafast pump-probe experiments revealed the intersystem crossing (ISC) mechanism (triplet-triplet transition) and the nonlinear absorption mechanism of the compound. The results indicate that this new phthalocyanine (**1**) can be considered a potential candidate for low-power OL applications.

1. Introduction

Phthalocyanines (Pcs) are of special class compounds with increasing interest for the mimic of novel functional materials due to their intrinsic properties, such as high thermal, photochemical, electrochemical stabilities and intense absorption in the UV-Vis and NIR region of the spectrum. The recent continued interest in these robust compounds mainly relies on their intended chemical, physical optical and electronic properties of which make them potential candidates for implementation in electrochromic materials, semiconductors, light-emitting diodes, sensors, nonlinear optical (NLO) materials, catalysts, and optical data storage systems, and as well as hole and electron transporting materials in perovskite solar cells [1,2]. The feasibility of these areas is related to their electron transfer properties. Therefore, the determination of the electrochemical features of new metallophthalocyanines (MPcs) is essential to identify the possibility of these usages in technological applications [3]. In the present study, the voltametric and spectroelectrochemical properties of **1** bearing hydroxyl groups at the peripheral positions were investigated and compared with the literature.

The electronic, optical, electrochemical, and photophysical properties of Pcs and MPcs can be adjustable by differing the metal center and/or substitution at the peripheral and non-peripheral positions [4]. The structure of the Pc molecules which influences the aggregation of Pcs, determines the spectroscopic behavior of the resulting aggregates [1,4]. It is known that a good OL material needs high solubility in solution to prevent aggregate formation [5]. For this purpose, here we present the synthesis of a novel ZnPc exhibiting desired photophysical and electronic properties due to its improved solubility and organizing capabilities [6]. As well known, the functional groups on the periphery plays a critical role in ensuring the technological applicability of MPcs due to the increase in the solubility of these compounds [7]. As reported by Annemie Adrianes and co-workers, the electron-withdrawing and electron-donating substituents have a major effect on the spectroscopic, stability and electrochemical data, and also electron transfer abilities of Pcs [8]. The reactive functional groups, in particular, such as hydroxyl on the Pc molecules have been interesting target for further chemical modification on the Pc ring [9,10]. DFT calcu-

* Corresponding author at: Department of Chemistry, Faculty of Arts and Sciences, Zonguldak Bülent Ecevit University, TR-67100 Zonguldak, Turkey.
E-mail address: sengul@beun.edu.tr (A. Şengül).

https://doi.org/10.1016/j.molstruc.2022.134046
0022-2860/

lations showed that MPcs bearing hydroxyl groups at the peripheral positions form stable J-dimers due to the intermolecular hydrogen bonds between the H atom of an OH group and the isoindole N atom of neighboring one [11]. These intermolecular interactions, such as hydrogen bonding and/or coordination bonds between the complexing metal ions and oxygen atoms of the OH groups determine the degree of aggregation, and usually enhance the NLO properties [9,11]. As we known, the presence of the polar substituents on the periphery of Pcs greatly influences the packing of the molecules through hydrogen bonds which significantly alter the physical properties that enhance their technological usage [12,13].The effective use of Pcs and their analogues in the above technological areas is restricted in some cases due to the dimerization of Pc molecules which may even lead to the formation of larger and more complex aggregates. However, in the present case, the introduction of four bulky substituents, 4,4-(octahydro-4,7-methano-5H-inden-5-ylidene)bisphenol at the peripheral positions should greatly enhance the solubility of Pc and inhibit aggregation process [14]. Hence, as demonstrated by H. Manaa et al, the aggregation behavior of Pcs can greatly affect the electrochemical and nonlinear optical properties by reducing the active absorbing excited-state lifetime [8,15].

The substitution of electron-donating or electron with-drawing group can result in the formation of aggregate species and can also induce intramolecular charge transfer, which has found its use in various electrochemical-based technological usages [16,17] as the driving force. In addition, the electron transfer abilities of phthalocyanines depend on the nature of the element in the inner core [18]. Thus, this paper also deals with the voltammetric and in situ spectroelectrochemical characterization of these complexes, which contains electron-donor substituents, the incorporation of Zinc metal center.

The progressing of optoelectronics technologies is related to the development of effective NLO materials [19]. Organic molecules attract considerable interest because of their fast response times, low fabrication costs and good NLO properties [20]. The NLO features of highly soluble monomeric and dimeric MPcs were examined [21–26]. Axial substituents prevent aggregation of the Pcs and change the electronic properties of Pcs because of the existence of an extra dipole moment positioned perpendicularly to the macrocycle [23]. Trimeric Pcs have great third-order nonlinearity due to intramolecular π–π interactions of Pc units as compared to monomeric and dimeric structures.

OL is a privileged property of the materials for NLO applications. Among the metallo organic frameworks, MPcs are notable functional materials because of binding to their chemical stability and conjugated π-electron system. OL properties increase with the peripheral alkoxy substituents [24–26]. The perfect properties of MPcs for OL applications occurred both their π-electron delocalization, chemical and thermal stability and their processability [27–29]. The reverse saturable absorption (RSA) is a dominant mechanism for OL in MPcs. In this mechanism large absorption cross-section ratio of triplet state to the ground state and triplet-triplet absorption have a critical role due to large pulse duration (nanosecond laser pulses) [30]. It is the first study that nonlinear absorption properties, OL properties, and charge transfer mechanisms of **1** investigated in THF.

2. Experimental

2.1. Materials

Synthetic grade reagents and solvents were used and all were sourced from commercial suppliers. Solvents and reagents were purified by the standard methods under an inert gas atmosphere. 4-nitrophthalonitrile and 4,4-(octahydro-4,7-methano-5H-inden-5-ylidene)bisphenol were supplied from Acros, 2-(dimethylamino)ethanol (DMAE) was supplied from ABCR, Zinc acetate, $Zn(OAc)_2{\bullet}2H_2O$ was supplied from Merck and 1,8-Diazabicyclo[5.4.0]undec-7-ene (DBU) was supplied from Aldrich. Thin layer chromatography (SiO_2) was used to test the purity of the products. Column chromatography was performed on silica gel 60.

2.2. Equipment

FT-IR (ATR) spectra were measured with a Perkin Elmer FT-IR Spectra 100 Spectrophotometer at room temperature. The ^{1}H NMR and ^{13}C DEPT NMR in $CDCl_3$ and THF-d_8 with an Agilent 600 MHz Premium Compact NMR spectrometer were used at room temperature. Chemical shifts were expressed in parts per million with reference to TMS. Mass spectra were recorded on a Rapiflex MALDI-TOF-MS (Bruker Daltonics, Bremen-GERMANY) with a Smartbeam 3D 10kHz 355 nm Nd: YAG laser was up to 1000 shots per sample spot with a single-shot laser configuration. For the MALDI matrix solution preparation, 10 mg/mL 2,5-dihydroxybenzoic acid MALDI matrix was prepared in 1:1 ACN:H_2O by v/v and acidified with trifluoroacetic acid (final acid concentration is 0.1%). **1a** was dissolved in acetonitrile (1 mg/mL) and mixed MALDI matrix solution in 1:10 volume ratio. For **1**, the same solution and the same concentration were prepared but this solution is directly deposited onto the MALDI target without mixing by MALDI matrix solution (LDI mass spectrum was acquired). All the final sample solutions were applied onto the MALDI target about 0.5 mL, dried at ambient temperature under air and then analyzed. For the mass calibration of MALDI-TOF-MS, peptide standard (Bruker-Germany) was used. The UV-Vis spectral measurements were performed with a SHIMADZU UV-Visible spectrophotometer. Fluorescence spectra were recorded on a HITACHI F-7000 Fluorescence spectrophotometer. All measurements were performed using freshly prepared solutions.

2.3. Synthesis

2.3.1. Phthalonitrile ***1a***

To the solution of 4-nitrophthalonitrile (4.10 g, 23.40 mmol) in anhydrous DMF (25 ml) 4,4-(octahydro-4,7-methano-5H-inden-5-ylidene)bisphenol (5.00 g, 15.60 mmol) were added under argon atmosphere. After stirring for homogenous solution, anhydrous K_2CO_3 (9.70 g, 70.20 mmol) was added in portion wise in 2 h. Then the reaction mixture was stirred overnight at room temperature. The mixture was then poured into 200 ml of ice-cold water. By column chromatography, the precipitate was purified on silica gel using CH_2Cl_2/EtOH (100/1) as eluent. Yield 2.0 g (29%). IR (ATR) ν, cm^{-1}: 3424, 3074, 3038, 2945, 2861, 2233, 1699, 1608, 1590, 1563, 1500, 1485, 1449, 1424, 1358, 1311, 1281, 1248, 1207, 1174, 1113, 1088, 1064, 1012, 979, 952, 879, 828, 767, 736, 702. HR MALDI-TOF MS (*m/z*): 601.166 $[M+Matrix+H]^+$ for $C_{30}H_{26}N_2O_2$+Matrix+H (MALDI matrix-2,5-dihydroxybenzoic acid:$C_7H_6O_4$) calcd. 601.233;. ^{1}H NMR (600 MHz, $CDCl_3$, Me_4Si): δ_H, ppm 7.68 (m, 1H), 7.38 (d, 1H), 7.34 (d, 1H), 7.19 (m, 4H), 6.90 (t, 2H), 6.72 (t, 2H), 4.78 (d, 1H), 2.89 (d, 1H), 2.35 (m, 1H), 2.28 (m, 1H), 2.23 (d, 1H), 2.15 (t, 1H), 1.82 (m, 4H), 1.54 (m, 1H), 1.43 (m, 1H), 1.24 (m, 1H), 1.10 (m, 2H), 1.04 (m, 1H), 0.87 (m, 1H). ^{13}C NMR (DEPT, 600 MHz, $CDCl_3$): δ_C, ppm (C) 153.173, 152,882, 150.737, 140.177, 117.525, 115.410, 115.004, 108.621, 54.796 (CH) 135.296, 129.204, 121.502, 121.395, 120.023, 119.855, 115.104, 49.478, 47.792, 42.390 (CH_2) 43.487, 27.240, 27.217 (CH_3).

2.3.2. Phthalocyanine ***1***

A mixture of **1a** (0.12 g, 0.26 mmol) and $Zn(OAc)_2{\bullet}2H_2O$ (0.16 g, 0.78 mmol) was dissolved in dry DMAE (4 mL). Then DBU (3 drops) was added and the mixture refluxed and vigorous stirred

16 h under an argon atmosphere. Then 15 mL methanol poured into the cooled reaction mixture. After that the crude product was filtrated and washed with methanol. Purification of the blue precipitate was done by column chromatography on silica gel using CH_2Cl_2/THF (20/1) as eluent. Yield 0.04 g (30%). IR (ATR) ν, cm^{-1}: 3288, 3034, 2943, 2861, 1770, 1717, 1612, 1600, 1502, 1475, 14481394, 1363, 1336, 1309, 1264, 1229, 1172, 1113, 1089, 1043, 1012, 946, 891, 827, 748, 678. MALDI-TOF MS monoisotopic mass (*m/z*): 1848.643 $[M]^+$ for $C_{120}H_{104}N_8O_8Zn$ calcd. 1848.727. ^1H NMR (600 MHz, THF-d_8, Me_4Si): δ_H, ppm 9.01 (m, 8H), 7.84 (m, 8H), 7.30 (m, 22H), 6.92(d, 4H), 6.64 (m, 6H), 3.02 (m, 4H), 2.50 (s, 6H), 2.40 (s, 2H), 2.34 (m, 2H), 2.27 (m, 2H), 2.18 (m, 2H), 2.10 (m, 2H), 1.97 (m, 2H), 1.83 (m, 4H), 1.61 (m, 6H), 1.53 (m, 4H), 1.46 (m, 2H), 1.40 (m, 4H), 1.29 (m, 4H), 1.23 (m, 4H), 1.12 (m, 4H), 0.93 (m, 2H). ^{13}C NMR (DEPT, 600 MHz, THF-d_8): δ_C, ppm (C) 169.396, 164.737, 158.561, 157.059, 156.737, 144.354, 140.246, 56.359 (CH) 131.227, 130.537, 129.625, 129.480, 121.066, 120.774, 116.514, 51.240, 49.899, 44.374 (CH_2) 45.156, 33.814, 33.454, 31.477, 28.895 (CH_3). UV-Vis (THF): λ_{max}, nm (log ε): 680 (5.03), 612 (4.31), 322 (5.06).

2.4. Computational details

Gaussian09 [31] was used for geometry optimization applying DFT [32–34] using Becke's 3 parameter exchange and Lee-Yang-Parr correlation (B3LYP) [35] functional combined with 6-31G(d,p) and LANL2DZ [36] basis sets. Visualizations were performed with Gaussview5.0 [37]. Frequency calculations at the same level were carried out and all optimized structures were verified as true minima. To calculate UV-Vis absorption spectra (n = 40 states) and molecular orbital energies, TD-DFT calculations were done using ground state optimized geometries. The TD-DFT calculations were also performed with B3LYP [35] and were repeated with CAM-B3LYP (Coulomb-Attenuating Method) [38] functional with 6-31G(d,p) and LANL2DZ [36] basis sets to have UV-Vis spectra. Experimental UV-Vis absorption spectra were compared with computational results. All calculations were done in solution to model the real systems. Solvent effects on the electronic transitions in DMF were investigated using Polarizable Continuum Model (PCM) [39] in all DFT and TD-DFT calculations.

2.5. *Electroanalytical,* in situ *spectroelectroanalytical, and* in situ *spectroelectrocolorimetric measurements*

The aim to display electrochemical and electrocolorimetry supported spectroelectrochemical measurements a Gamry Reference 600 model potentiostat/galvanostat was employed. Cyclic voltammetry (CV) and square wave voltammetry (SWV) measurements, the analyte, i.e., the solution of a Pc compound in extra pure DMSO involving electrochemical grade tetrabutylammoniumperchlorate (TBAP) as the supporting electrolyte at a concentration of 0.10 mole dm^{-3} was placed in a cell with three electrode configuration at 25°C. A Pt and a Pt spiral wire were used as the working and counter electrodes, respectively, while a saturated calomel electrode (SCE) was treated as the reference electrode. The analyte solution was deoxygenated for fifteen minutes prior to each run by the high purity of N_2. Also, electrocolorimetry supported spectroelectrochemical measurements was followed, as the procedure described in the literature [1].

2.6. NLO measurements

The nonlinear absorption measurements of the studied compounds were researched by the OA Z-scan technique. This technique measures the total transmittance through the sample depending on the intensity around focal length of the lens (20 cm focal length). A Q-switched Nd:YAG laser (Quantel Brillant) with 10 Hz repitation rate, 4 ns pulse duration and 532 nm wavelength was used. Z-scan experiments were conducted in quartz cuvettes with 1 mm path length in solution environment. The linear absorption coefficients of compound is 1.07 cm^{-1}. In order to understand intersystem crossing (ISC) mechanism and excited states dynamic of the compound ultrafast pump-probe spectroscopy measurements were carried out with femtosecond laser system. The detail information about the experimental procedure for pump-probe and nonlinear absorption measurements were given in the literature [1].

3. Results and discussion

3.1. Synthesis and characterization studies

The precursor compound, phthalonitrile **1a** was synthesized by the reaction of 4,4-(octahydro-4,7-methano-5H-inden-5-ylidene)bisphenol with 4-nitrophthalonitrile which is shown in Scheme 1. The disappearance of the characteristic NO_2 stretching bands while the formation of nitrile peaks evidenced the formation of **1a**. The nitrile peaks appear at 2233 cm^{-1} and the C-O-C peaks at 1207 cm^{-1}, respectively (Fig. S1 in ESI). In the HR MALDI TOF mass spectrum of **1a**, a major peak at *m/z* 446.35 $[M]^+$ proves the structure (Fig. S2 in ESI). The ^1H NMR spectrum of **1a** (Fig. S3 in ESI) is consistent with the proposed structure as depicted in Scheme 1. The doublets of phthalonitrile aromatic protons appear at 7.68-6.72 ppm. The hydroxyl of the phthalonitrile appear at 4.78 ppm. The phthalonitrile aliphatic protons appear in a range of multiplets over 2.89-0.87 ppm. The ^{13}C DEPT NMR spectrum of **1a** (Fig. S4) give the characteristic signals regarding the number of attached carbons to each other in the molecule as of primary carbons, secondary carbons, tertiary carbons, and quaternary carbons in their respective regions as evidence by the number of primary carbons, secondary carbons, tertiary carbons, and quaternary carbons at the molecule.

The formation of **1** is proved by the disappearence of the C≡N stretching at 2233 cm^{-1} (Fig. S5 in ESI). The purified **1** was further characterized by HR MALDI TOF mass spectra (Fig. S6 in ESI). The mass spectra reveal a molecular ion peak at *m/z* 1850.66 $[M]^+$ which is well-matched with the calculated value. The ^1H NMR spectrum of **1** (Fig. S7) is consistent with the optimized structure. Unfortunately, the spectrum is not very well resolved as common to Pcs of those having extensive intermolecular interactions and also due to presence of statistical isomers in solution. However, we can readily determine the proton integral ratio and values which are in good consonance with the suggested molecular formula. The assignment of the protons shows that the aromatic protons appear in the aromatic region over 9.01-6.64 ppm, and the aliphatic protons over 3.02-0.93 ppm as predicted. The broadness of the peaks in the ^1H NMR spectra is usually caused by the aggregation–disaggregation equilibrium and the formation of H-bonds between the hydroxyl groups on the Pc [40]. The ^{13}C DEPT NMR spectrum of **1** (Fig. S8) clearly confirms the structure of molecule.

3.2. Electronic absorption and fluorescence emission studies

At different concentrations (1.0×10^{-5} to 1×10^{-6} M) the aggregation behavior of **1** was studied in DMF (Fig. S9). At high concentrations, the intensity of the absorption tends to increase. Besides no new bands appear because of the aggregation. Result indicates that absorbance varies with concentration, this result is consistent with Beer-Lambert Law. The electronic absorption spectrum of **1** include characteristic B and Q bands which is typical for MPc complexes. The ZnPc **1** shows B and Q bands at 322 nm and 680

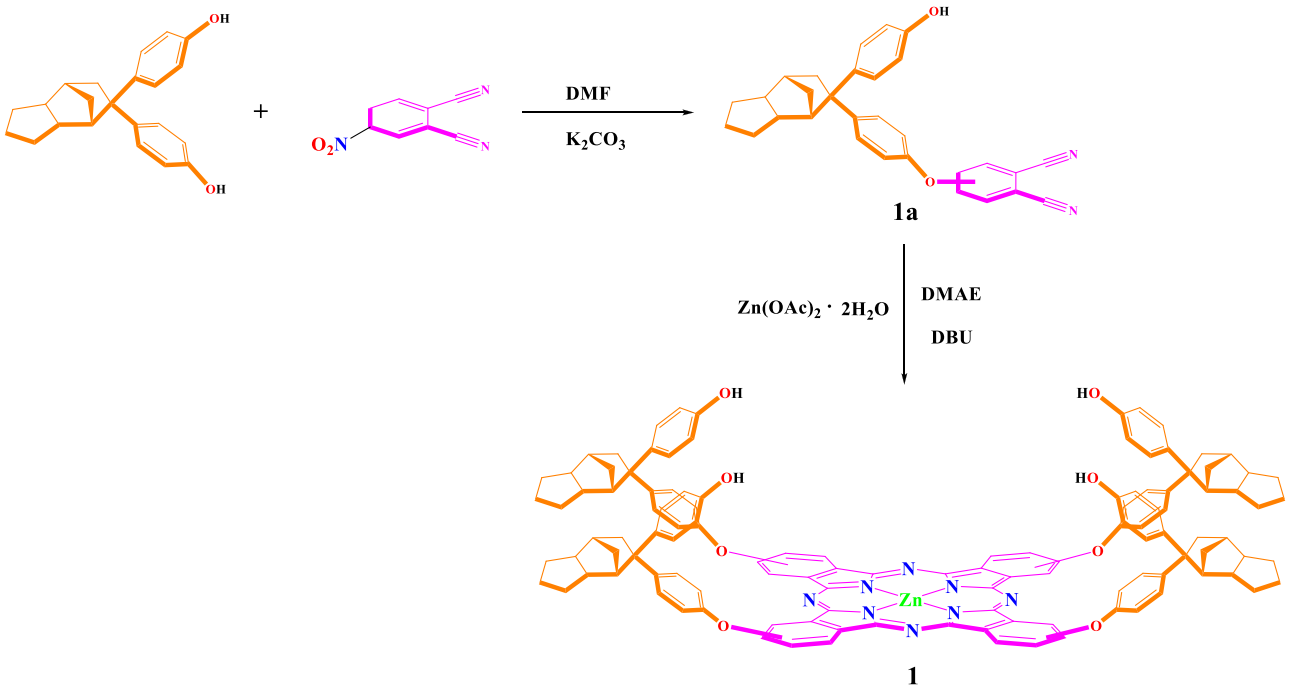

Scheme 1. The synthetic route toward **1**.

nm, respectively. The fluorescence behaviors (absorption, fluorescence emission, and excitation spectra) of **1** were studied in DMF (Fig. S10).

3.3. Computational results

The optimized structure for **1** is shown in Fig. 1 and Fig. S11 with different views in DMF. Some bond distances, bond angles, dihedral angles, dipole moments (μ), and the sum of electronic energies with zero-point energy corrections (E_{elec}+ZPE) of the compound calculated at B3LYP/6-31G(d,p)/LANL2DZ in DMF, are listed in Table S1.

Although the molecule appears to be symmetrical, 4,4-(octahydro-4,7-methano-5H-inden-5-ylidene) bisphenol groups showed small deviations from the plane of the molecule. The middle polarity value of the dipole moment supports this situation. The ZnPc core keeps its square-planar structure (90° for N1-Zn-N2). The torsion angle (C1-O1-C2-C3) between the benzene rings bound to oxygen (O1) and Pc is 65.7º and the bond angle C1-O1-C2 is 120.4º. The groups attached to C5 have a tetrahedral geometry.

Molecular electrostatic potential surface (MEP) map was calculated to investigate the electron distribution on the molecular surface showing the active regions for electrophilic and nucleophilic attacks. Red color implies the negative charges and the blue color shows the positive charges. According to Fig. 1B, electron density on the molecular surface is at the oxygen atoms on octahydro-4,7-methano-5H-inden-5-ylidene)bisphenol groups and the nitrogen atoms in the Pc core. The positive charge (blue color on H) and the negative charge (red color on the oxygen) in the OH group indicate polarity. Therefore, the molecule has active interaction sites.

The HOMO (highest occupied molecular orbital) and LUMO (lowest unoccupied molecular orbital) are localized on Pc (Fig. 1C). The value of energy difference between the HOMO and LUMO is 2.13 eV for **1** in DMF. This low energy gap facilitates the charge transfer transitions.

TD-DFT calculations at B3LYP/6-31G(d,p)/LANL2DZ and CAM-B3LYP/6-31G(d,p)/LANL2DZ levels were carried out to calculate the absorption wavelengths and excitation energies for the first 40 singlet excited states for **1**. The CAM-B3LYP values are more in line with the experimental results in THF (Fig. S12). Fig. 2 shows the calculated UV-Vis absorption spectra of **1** with oscillator strength in THF.

Characteristic Q bands (687.2 nm and 684.4 nm) and B bands (321.0 nm and 320.7 nm) with high oscillator strength display local excitation of the Pc (LE) from HOMO to LUMO and from HOMO-8 to LUMO, respectively (Table S2, Fig. S13). These transitions are in good agreement with the experimental results in terms of wavelength and absorptivity (ε). Intramolecular charge transfer (ICT) from the benzene and the phenol rings to the Pc (CT1) observed with low oscillator strength between 349.9 nm and 280.2 nm. Additionally, both LMCT (ligand-to-metal charge transfer) and local excited (LE) Pc are observed at 286.9 nm. ICT from the Pc to benzene rings (CT2) is at 277.6 nm from HOMO to LUMO+5 orbitals. The single bonds in octahydro-4,7-methano-5H-inden-5-ylidene)bisphenol groups also participate in CT at 252.1 nm (CT3: ICT from octahydro-4,7-methano-5H-inden-5-ylidene)bisphenol groups to the Pc).

3.4. Electrochemistry

The voltammetric analysis of **1** has been identified by CV and SWV and electrocolorimetry supported *in situ* spectroelectrochemistry in a non-aqueous solvent containing organic metal salt on a Platinum working electrode. Table 1 lists the relevant electrochemical data, which includes the half-wave potential ($E_{1/2}$), the anodic to cathodic peak potential separation (ΔE_p), the peak currents ratios (I_{pa}/I_{pc}), and the difference between the first oxidation and reduction potentials ($\Delta E_{1/2}$) for the relevant redox couple (except the first oxidation and reduction processes due to split ill-defined redox signals). On the other hand, the voltametric responses of **1** are compared with the similar peripheral analogues reported by our group [41] and unsubstituted Pcs in the literature [42]. As the electrochemical data consider that redox processes have been shifted usually toward more positive potentials. This positive potential shift can be recognized to the electron-releasing nature of

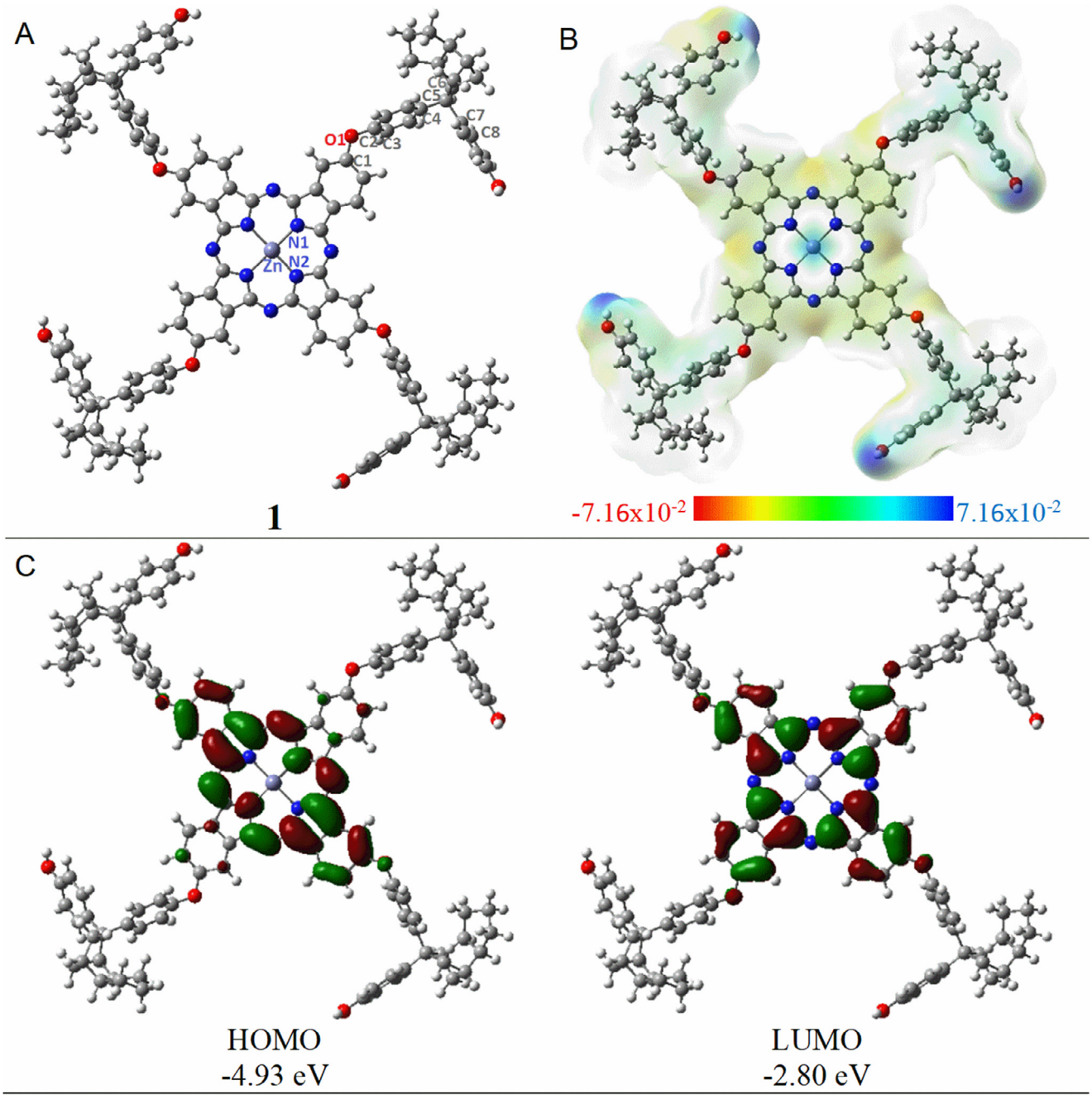

Fig. 1. (A) Optimized stable geometry, (B) molecular electrostatic potential surface (MEP) map and (C) HOMO, LUMO for **1** in DMF (isovalue is 0.02 a.u.). (Red: electron-rich; yellow: slightly electron-rich; green: neutral; light blue: slight electron deficiency; blue: electron deficiency in MEP).

Table 1
The electrochemical data for the peripherally-substituted Pc compound **1** and comparison with close analogs.

Pcs	Label	O2	O1'(O1'')	R1'(R1'')	R2	R3	$DE_{1/2}$ (V)	Ref.
ZnPc (1) in DMSO	[a]$E_{1/2}$ (V)	-	0.73[f] (0.94[f])	-0.56[e] (-0.79[e])	-1.40	-		
	[b]DE_p (mV)	-	-	-	70		1.29[d]	Tw[g]
	[c]I_{pa}/I_{pc} (V)	-	-	-	0.96			
ZnPc in DMSO	[a]$E_{1/2}$ (V)	1.06	0.96	-0.55 (-0.70)	-0.81 (-1.07)	-1.65	1.51[d]	[41]
ZnPc	[a]$E_{1/2}$	-	0.67	-0.86	-1.30	-1.85		[42]

[a] $E_{1/2}=(E_{pa}+E_{pc})/2$ at 0.100 Vs^{-1}.
[b] $\Delta E_p= E_{pa}-E_{pc}$ at 0.100 Vs^{-1}.
[c] I_{pa}/I_{pc} for reduction, I_{pc}/I_{pa} for oxidation processes at 0.100 Vs^{-1} scan rate.
[d] $\Delta E_{1/2} = E_{1/2}$ (first oxidation) - $E_{1/2}$ (first reduction). HOMO–LUMO gap for MPc having an electro inactive metal center.
[e] It could not be determined for some redox processes due to ill-defined redox waves.
[f] These redox couples could be detected only by square wave voltammetry.
[g] This study.

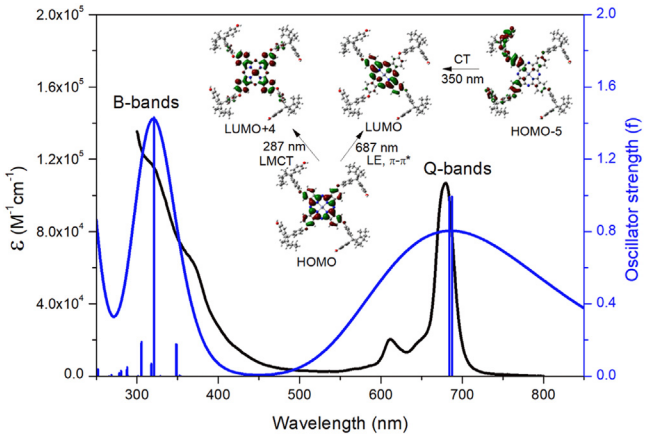

Fig. 2. Calculated and the experimental (black line) UV-Vis absorption spectra of **1** in THF.

the peripheral substituents. Furthermore, according to literature and the peak positions and $\Delta E_{1/2}$ value for **1** show only Pc based one-electron transfer reactions due to the presence of an inactive metal center [18]. However, the first processes given the initial oxidation and reduction are divided into two waves. This can be explained by the aggregation-disaggregation equilibrium of the complexes. CVs and SWVs of **1** are shown in Fig. 3A as representative examples. Fig. 3A represents CVs and SWVs of ZnPc in DMSO/TBAP on a Pt working electrode. During potential scans to the cathodic side, two processes are observed. The former one due to the aggregation the first reduction process is split into two process, at R1' (-0.56 V) and R1" (-0.79 V), which are marked a small wave. These split reduction reactions seem electrochemically quasi-reversible concerning for to the complication of aggregation phenomenon of compound **1**. Thus, the ΔE_p, and the I_{pa}/I_{pc} couldn't been determined.

However, the chemical irreversibilities of the first electron transfer processes can be identified by the presence of the equilibrium between the aggregated and nonaggregated ZnPc species. After the first reduction process, the complex is disaggregated, therefore the latter process, R2, has high peak current than those of the former one. ZnPc also illustrates splitted oxidation process (O1' and O1"), which is identified by square wave voltammetry alone. The aggregation-disaggregation equilibrium of the complexes also influences the oxidation process by splitting the process into two waves at 0.73V and 0.94 V. The measured redox behaviors may be observed at slightly low current values in CV measurements due to the aggregated species in the bulk solution. In addition, CV technique sometimes usually have a lower sensitivity due to the large capacitive contribution that is not observed in the DPV or SWV [43]. In order to better determine these the aggregation-disaggregation equilibrium, all redox pairs also characterized by the pulse voltammetry technique (SWV) clearly as given Fig. 3A. SWV technique makes the peaks that we see as relatively weak in CV more understandable.

With the aim of assigning the redox processes to the Pc ring electron transfer ability, the spectroelectrochemical measurements of **1** were carried out in during the electrolysis of the solution of **1** in DMSO/TBAP electrolyte system at -1.10 V constant potentials vs. SCE in DMSO/TBAP. (Fig. 3B-D). The spectral changes corresponding to the first reduction process are divided into two following groups. Fig. 3B and C represent to confirm additional support for the identification of possible aggregation effects. As shown in Fig. 3B, the original form of **1** indicates that the main Q-band absorption at 679 nm and with a shoulder at 618 nm and B band at 347 nm. However, the green band at 618 nm in the original spectrum is characteristic for the presence of a aggregation-disaggregation equilibrium of the complexes [41]. During the first spectral changes for the reduction processes, while the intensity of the Q-band absorption at 678 nm increases without shift the B band intensity decrease under at -1.10 V potential and net isobestic points at 406, 632 and 714 nm appear. These spectral changes clearly indicate that the aggregation equilibrium shifted towards the monomer species prior to the ligand based first reduction process. End of these spectral changes the original green color of the solution turned to blue (Fig. 3D). Upon the latter reduction at -1.10 V, the intensity of the Q-band absorption decreases without shifting and a new band is observed at 575 nm as seen in Fig. 3C. The Pc ring-based assignment of the second reduction of complex **1** in Table 1 is supported by these UV-Vis spectral changes. Furthermore, after the reduction processes, it turns to deep blue as shown in the chromaticity diagram (Fig. 3D).

3.5. Nonlinear absorption properties

The UV-Vis absorption spectra are given in Fig. 4. The absorption bands are localized at 675 nm, 610 nm, 355 nm, and 270 nm in THF solution. The dilute solution spectrum of **1** in Fig. 4, does not show agglomeration, however at higher concentrations in THF solution, the aggregation occurs significantly as shown in Fig. 4. Since the both monomer and aggregate absorption peaks are overlapped, a broad peak is observed in the absorption spectrum at the high concentration in THF.

The nonlinear absorption characteristics of **1** in THF were examined by OA Z-scan technique [44]. Fig. 5 indicates the OA Z-scan experimental results with different input intensities. The normalized transmission decreased towards to focus and this behavior indicates intensity-dependent absorption. The following equation gives the normalized transmittance T_{norm} (z) as a function of z position [44].

$$T_{norm}\ (z) = \frac{log_e[1 + q_0(z)]}{q_0(z)}$$

In the above equation, q_0 (z) is given by,

$$q_0(z) = \frac{q_{00}}{1 + (z/z_0)^2},\ q_{00 \sim \beta_{eff} I_0 L_{eff}}$$

where β_{eff} is the effective coefficient of nonlinear absorption, I_0 is the intensity of the light at focus, and z_0 is the diffraction length of the beam. $L_{eff} \sim [1-exp(-\alpha_0 L)]/\alpha_0$, is the effective length of the sample and defined in terms of the true optical path length through the simple, L and linear absorptivity, α_0. The method of least-squares regression was used to all OA Z-scan experimental results.

The OL properties of the studied compounds were extracted from OA Z-scan experimental data. It was reported in the previous study, the reverse saturable absorption (RSA) from excited triplet state absorption enhanced OL of **1** in THF [45]. By absorbing a photon, each molecule at the ground state (S_0) state excites the S_1 state and these electrons may excite to upper electronic state via excited state absorption (ESA), relax to ground state with radioactive or nonradioactive decay, or transfer to T_1 state via the ISC mechanism. In RSA mechanism, the excided state absorption cross section value both for S_1 and T_1 state is larger than that of ground state. The nonlinear absorption coefficient derived from rate equations and steady-state approximation [22,45] is given the following equation.

$$\alpha(I,\ I_{sat},\ \kappa) = \frac{\alpha_0}{1 + \frac{F}{F_{sat}}}\left(1 + \kappa\frac{F}{F_{sat}}\right)$$

κ is the ratio of the triplet state to ground state absorption cross-section, α_0 is the linear absorption coefficient and F_{sat} is the saturated value of the output energy density. κ and F_{sat} parameters

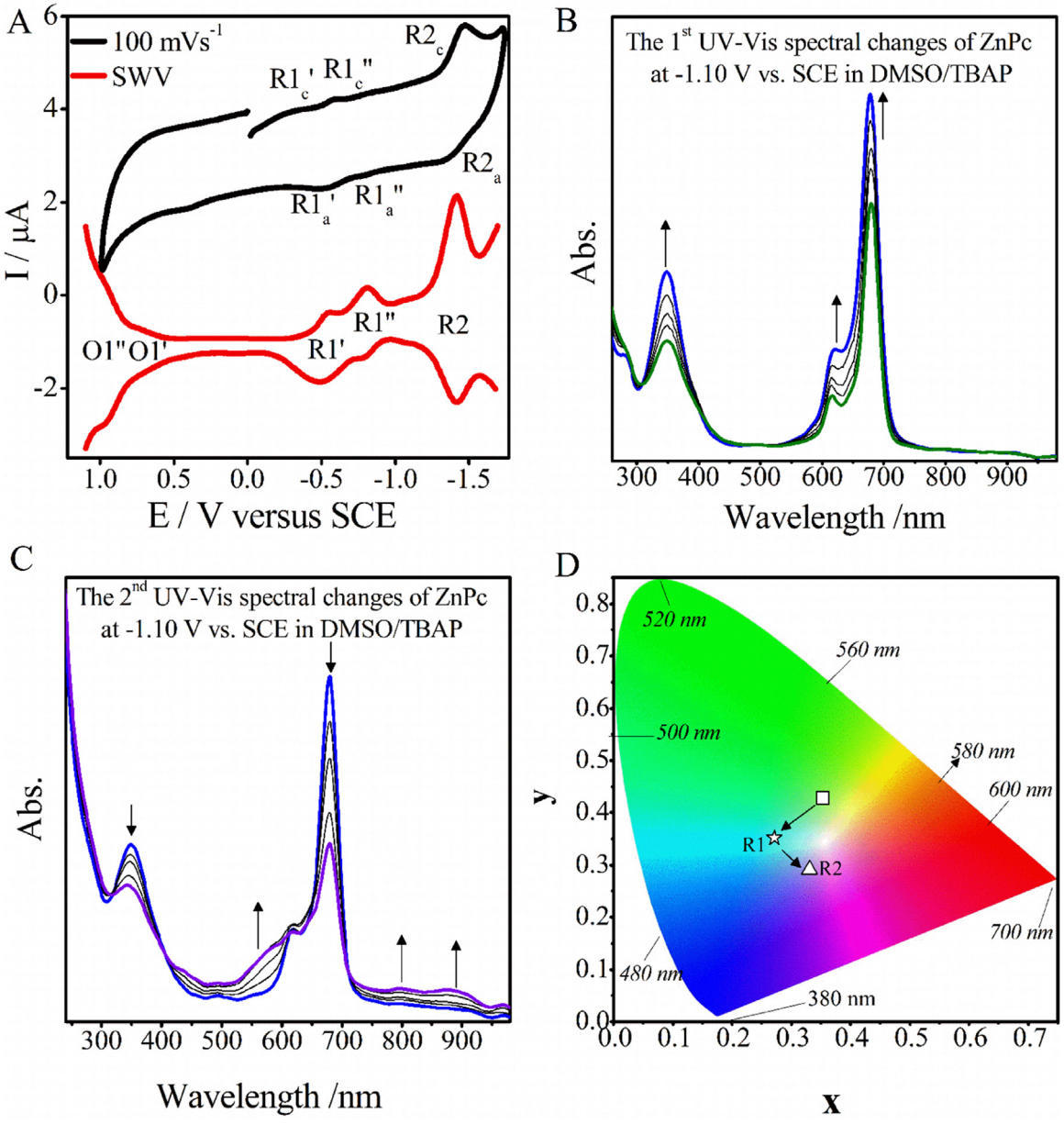

Fig. 3. (A) Cyclic and square wave voltammograms of 5.0 × 10^{-4} mol dm^{-3} **1** in TBAP/DMSO. (B) The first and (C) the second groups of *in situ* UV–Vis spectral changes throughout the controlled potential electrolysis of **1**. (D) chromaticity diagram for **1** in DMSO/TBAP.

were used as free constants. The OL graph is given in Fig. 6 depending on the incident energy density per pulse. The materials possessing high OL properties must have high κ, β_{eff} and low F_{sat}, α_0 values. κ is significantly sensitive to linear absorption coefficient and the concentration of the solution [22]. The NLO parameters (β_{eff}, F_{sat}, κ) of **1** in THF solution are calculated as 7.5 × 10^{-8} cm/W, 10.2 J/cm^2, 5.4 for β_{eff}, F_{sat} and κ, respectively, from the fitting experimental results respectively. The OL parameters are convenient with literature [1]. Blau and co-workers presented the values of optical limiting parameters of structurally different phthalocyanine derivatives containing Zn^{II}, Co^{II}, Ni^{II}, Pd^{II}, Ga^{II}, and In^{III} metal atoms manipulated by the Z-scan technique [28]. In this study, CoPc or NiPc monomers are found out to be the weakest nonlinear absorbers among the 39 different kinds of investigated Pc compounds. In a review [20], optical limiting parameters (β_{eff}, F_{sat}, and κ) are taken into account for 39 materials. In this review, it was found that β_{eff} ranges in the order of 10^{-10} to 10^{-8} cmW^{-1}, F_{sat} in the order of 1 to 170 J cm^{-2}, and κ in the order of 1 to 27 [22]. On the other hand, for the polymeric films, β_{eff} ranges in the order of 10^{-4} to 10^{-6} cmW^{-1}, F_{sat} in the order of 1.6–20.2 J cm^{-2} and κ in the order of 3.2–23.8 [46–49]. Comparing with the literature the investigated ZnPc in THF solution shows a very good combination between a very high effective nonlinear absorption coefficient β_{eff}, a relatively high absorption cross-section κ, a very low energy-dependent saturation F_{sat} and is a good candidate as an optical limiting material.

Femtosecond transient absorption spectroscopy experiments were also conducted to determine whether there is a triplet transition or not. The pump wavelength was chosen as 675 nm corresponding to Q band of the sample. Fig. 7 shows the transient absorption spectra with different time delay for **1** in THF. In transient absorption spectra of **1**, there is an intense negative signal around 675 nm corresponding to ground state bleaching and wide excited state absorption (ESA) signal under 600 nm and above 720 nm

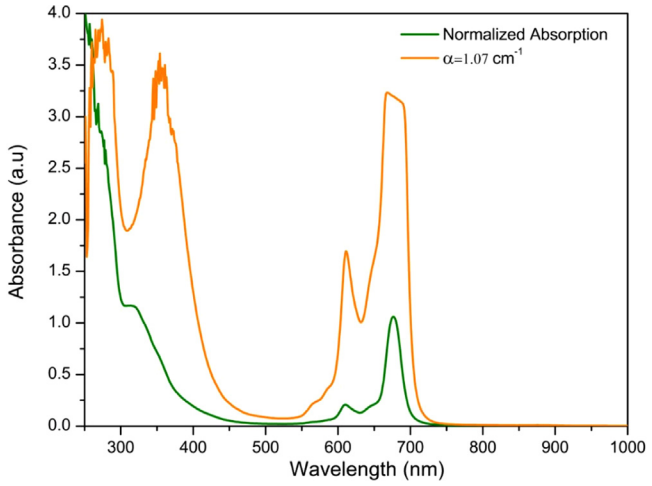

Fig. 4. Linear absorption spectra of **1** in THF solution α=1.07 cm^{-1} at 532 nm wavelength which is used for OA Z-scan experiments.

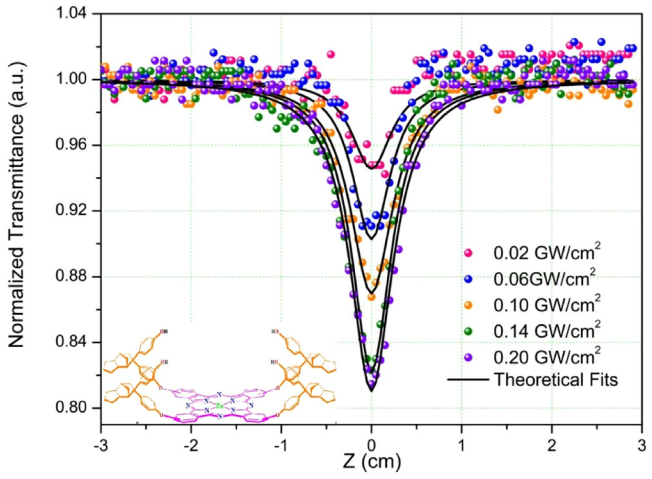

Fig. 5. Open-aperture Z-scan traces of **1** with different input intensities.

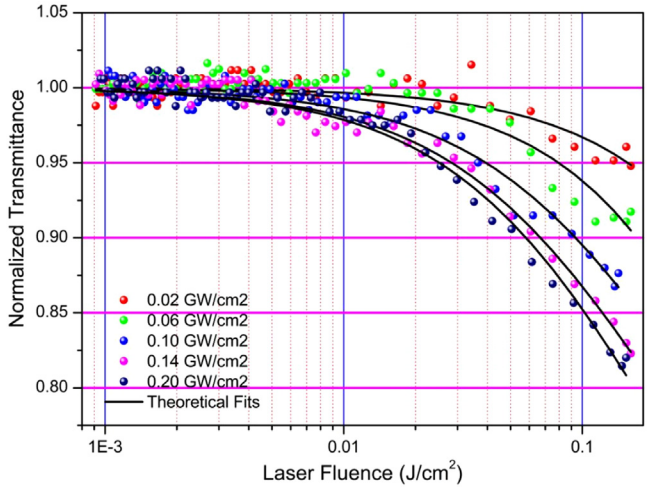

Fig. 6. OL properties of **1** with different input intensities in THF, λ_{ex} = 532 nm.

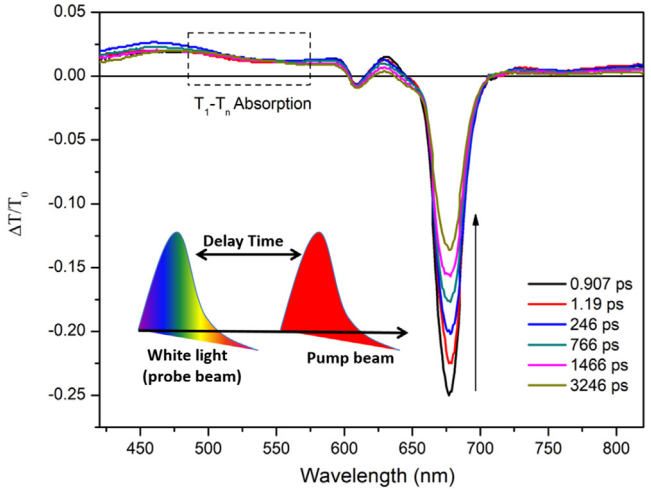

Fig. 7. Transient absorption spectra of **1** with different time delays at the excitation wavelength of 675 nm.

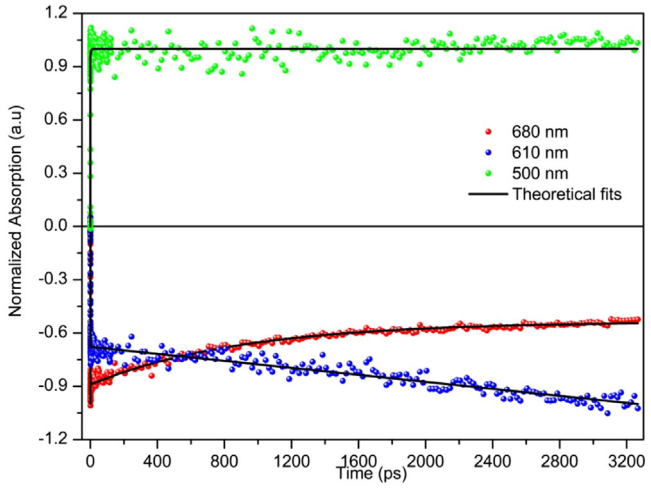

Fig. 8. Decay traces of **1** at 500 nm, 610 nm, and 680 nm probe wavelength with 675 nm excitation.

region. Similar transient absorption characteristic behaviors were also demonstrated for **1** [50]. Since the ESA signals in the range of 500 nm - 550 nm have very long lifetime components by probing 500 nm wavelength, these signals can be ascribed to the triplet-triplet transition, as seen in Fig. 8. In addition to that, the intensity of the bleach signal at 675 nm decrease while increasing the intensity of the 610 nm bleach band. It is shown that the electron transfer occurs between two bands. According to the decay kinetics of these two bands in Fig. 7, the symmetric traces are seen for 610 nm and 680 nm probe wavelengths.

4. Conclusions

In this work, we have thoroughly investigated the optical, spectrochemical, DFT and TD-DFT and the NLO properties of the peripherally tetrahydroxy-substituted ZnPc. The calculated results show that O and H atoms on the phenol groups will be active in the interactions. The electron transfer properties of **1** were investigated by voltammetry. A general tendency for the complex was their aggregation character, suggested by splitting or broadening of the redox waves. The electrochemical measurements verified that **1** possess a ligand-based one-electron redox processes, which are affected by the formation of aggregated species in the solution medium. The nonlinear absorption experimental results show that

1 has a strong reverse saturable absorption feature. The investigated compound is a promising material for OL applications due to its excellent combination (low α_0, high β_{eff}, high κ, and low F_{sat}) of OL parameters. The DFT and TD-DFT calculations support the experimental results. Femtosecond transient absorption spectroscopy results revealed an ISC process and nonlinear absorption mechanism.

Declaration of Competing Interest

The authors declare that they have no known competing financial interests or personal relationships that could have appeared to influence the work reported in this paper.

CRediT authorship contribution statement

Sebile Işık Büyükekşi: Investigation, Methodology, Validation, Writing – review & editing. **Efe Baturhan Orman:** Methodology, Validation, Visualization. **Ahmet Karatay:** Methodology, Visualization, Validation. **Nursel Açar Selçuki:** Data curation, Software, Visualization, Validation. **Ali Rıza Özkaya:** Methodology, Visualization, Validation, Data curation. **Ayhan Elmali:** Supervision, Methodology. **Bekir Salih:** Methodology, Validation. **Abdurrahman Şengül:** Conceptualization, Methodology, Validation, Resources, Data curation, Writing – original draft, Writing – review & editing, Visualization, Supervision, Project administration, Funding acquisition.

Data Availability

Data will be made available on request.

Acknowledgments

The authors thank Zonguldak Bülent Ecevit University for financial support under the project [BAP Project No: 2015-72118496-05]. Computer time on TUBITAK-ULAKBIM Truba resources are greatly acknowledged. Ali Rıza Özkaya and Bekir Salih also thank the Turkish Academy of Sciences (TÜBA) for partial support to this study.

Supplementary materials

Supplementary material associated with this article can be found, in the online version, at doi:10.1016/j.molstruc.2022.134046.

References

[1] S.I. Büyükekşi, A. Karatay, E.B. Orman, N. Açar Selçuki, A.R. Özkaya, B. Salih, A. Elmali, A. Şengül, A novel AB3-type trimeric zinc(ii)-phthalocyanine as an electrochromic and optical limiting material, Dalton Trans. 49 (40) (2020) 14068–14080.
[2] S.G. Makarov, O.N. Suvorova, C. Litwinski, E.A. Ermilov, B. Röder, O. Tsaryova, T. Dülcks, D. Wöhrle, Linear and rectangular trinuclear phthalocyanines, Wiley Online Library, 2007.
[3] M. Özdemir, S. Altinisik, B. Köksoy, B. Canımkurbey, S. Koyuncu, M. Durmuş, M. Bulut, B. Yalçın, New metallophthalocyanines including benzylphenoxy groups and investigation of their organic-field effect transistor (OFET) features, Dyes Pigments 200 (2022) 110125.
[4] T. Nyokong, Electronic spectral and electrochemical behavior of near infrared absorbing metallophthalocyanines, Funct. Phthalocyanine Mol. Mater. (2010) 45–87.
[5] B. Das, M. Umeda, E. Tokunaga, T. Toru, N. Shibata, Synthesis of benzene-centered trinuclear phthalocyanines by triple-click chemistry, Chem. Lett. 39 (4) (2010) 337–339.
[6] N. Ceylan, G. Gümrükçü, G.K. Karaoğlan, A. Gül, Synthesis, characterization, fluorescence spectra and energy transfer properties of a novel unsymmetrical zinc phthalocyanine with peripherally coordinated Ru (II) complex, Synth. Met. 206 (2015) 55–60.
[7] T. Nyokong, Effects of substituents on the photochemical and photophysical properties of main group metal phthalocyanines, Coord. Chem. Rev. 251 (13-14) (2007) 1707–1722.
[8] K.S. Lokesh, A. Adriaens, Synthesis and characterization of tetra-substituted palladium phthalocyanine complexes, Dyes Pigments 96 (1) (2013) 269–277.
[9] A.Y. Tolbin, M.S. Savelyev, A.Y. Gerasimenko, L.G. Tomilova, N.S. Zefirov, Thermally stable J-type phthalocyanine dimers as new non-linear absorbers for low-threshold optical limiters, PCCP 18 (23) (2016) 15964–15971.
[10] A.Y. Tolbin, V.E. Pushkarev, L.G. Tomilova, N.S. Zefirov, Threshold concentration in the nonlinear absorbance law, PCCP 19 (20) (2017) 12953–12958.
[11] A.Y. Tolbin, V.E. Pushkarev, L.G. Tomilova, N.S. Zefirov, Monohydroxyphthalocyanines as potential precursors to create nanoscale optical materials, J. Porphyrins Phthalocyanines 21 (02) (2017) 128–134.
[12] A.Y. Tolbin, A.V. Dzuban, V.I. Shestov, Y.I. Gudkova, V.K. Brel, L.G. Tomilova, N.S. Zefirov, Peripheral functionalisation of a stable phthalocyanine J-type dimer to control the aggregation behaviour and NLO properties: UV-Vis, fluorescence, DFT, TDHF and thermal study, RSC Adv. 5 (11) (2015) 8239–8247.
[13] Y. Bian, J. Chen, S. Xu, Y. Zhou, L. Zhu, Y. Xiang, D. Xia, The effect of a hydrogen bond on the supramolecular self-aggregation mode and the extent of metal-free benzoxazole-substituted phthalocyanines, New J. Chem. 39 (7) (2015) 5750–5758.
[14] L. Jian-Bo, Z. Fu-Qun, Z. Yu, Z. Fu-Shi, T. Ying-Wu, S. Xin-Qi, C. Footim, Substituent dependence of photophysical properties for free-base phthalocyanines, Acta Phys.-Chim. Sin. 12 (6) (1996) 491–495.
[15] H. Manaa, A. Tuhl, J. Samuel, A. Al-Mulla, N. Al-Awadi, S. Makhseed, Photophysical and nonlinear optical properties of zincphthalocyanines with peripheral substitutions, Opt. Commun. 284 (1) (2011) 450–454.
[16] S. Khene, T. Nyokong, Single walled carbon nanotubes functionalized with nickel phthalocyanines: effects of point of substitution and nature of functionalization on the electro-oxidation of 4-chlorophenol, J. Porphyrins Phthalocyanines 16 (01) (2012) 130–139.
[17] L. Jian-Bo, Z. Fu-Qun, Z. Yu, Z. Fu-Shi, T. Ying-Wu, S. Xin-Qi, C. Footim, Substituent dependence of photophysical properties for free-base phthalocyanines, ACTA Physico-Chimica Sinica 12 (6) (1996) 491–495.
[18] Edited by D. WöhrleC.C. Leznoff, A.B.P. Lever, Weinheim VCH (Eds.), Phthalocyanines: properties and applications, Adv. Mater. 5 (12) (1993) 942–943.
[19] J. Zyss, D. Chemla, Quadratic nonlinear optics and optimization of the second-order nonlinear optical response of molecular crystals, in: Nonlinear Optical Properties of Organic Molecules and Crystals, Elsevier, 1987, pp. 23–191.
[20] J.-L. Bredas, C. Adant, P. Tackx, A. Persoons, B. Pierce, Third-order nonlinear optical response in organic materials: theoretical and experimental aspects, Chem. Rev. 94 (1) (1994) 243–278.
[21] G. De La Torre, P. Vázquez, F. Agullo-Lopez, T. Torres, Role of structural factors in the nonlinear optical properties of phthalocyanines and related compounds, Chem. Rev. 104 (9) (2004) 3723–3750.
[22] S.M. O'Flaherty, S.V. Hold, M.J. Cook, T. Torres, Y. Chen, M. Hanack, W.J. Blau, Molecular engineering of peripherally and axially modified phthalocyanines for optical limiting and nonlinear optics, Adv. Mater. 15 (1) (2003) 19–32.
[23] G. Rojo, G. Martin, F. Agullo-Lopez, T. Torres, H. Heckmann, M. Hanack, Second-harmonic generation from axially substituted indium phthalocyanines, J. Phys. Chem. B 104 (30) (2000) 7066–7070.
[24] M. Sanghadasa, I.-S. Shin, R.D. Clark, H. Guo, B.G. Penn, Optical limiting behavior of octa-decyloxy metallo-phthalocyanines, J. Appl. Phys. 90 (1) (2001) 31–37.
[25] S. Qu, Y. Chen, Y. Wang, Y. Song, S. Liu, X. Zhao, D. Wang, Enhanced optical limiting properties in a novel metallophthalocyanine complex (C12H25O) 8PcPb, Mater. Lett. 51 (6) (2001) 534–538.
[26] Y. Chen, Y.-J. Li, S. Qu, Y. Song, Y.-X. Nie, D.-Y. Wang, Third-order optical nonlinearities and optical limiting of octa-octyloxy phthalocyanine free base in toluene, Opt. Eng. 40 (12) (2001) 2683–2684.
[27] D. Dini, M. Barthel, M. Hanack, Phthalocyanines as active materials for optical limiting, Eur. J. Org. Chem. 2001 (20) (2001) 3759–3769.
[28] C.G. Claessens, W.J. Blau, M. Cook, M. Hanack, R.J. Nolte, T. Torres, D. WoÈhrle, Phthalocyanines and phthalocyanine analogues: the quest for applicable optical properties, Monatsh. Chem. 132 (1) (2001) 3–11.
[29] Y. Chen, M. Hanack, W.J. Blau, D. Dini, Y. Liu, Y. Lin, J. Bai, Soluble axially substituted phthalocyanines: synthesis and nonlinear optical response, J. Mater. Sci. 41 (8) (2006) 2169–2185.
[30] C. Giuliano, L. Hess, Nonlinear absorption of light: optical saturation of electronic transitions in organic molecules with high intensity laser radiation, IEEE J. quantum electron. 3 (8) (1967) 358–367.
[31] M.J. Frisch, G.W. Trucks, H.B. Schlegel, G.E. Scuseria, M.A. Robb, J.R. Cheeseman, G. Scalmani, V. Barone, B. Mennucci, G.A. Petersson, H. Nakatsuji, M. Caricato, X. Li, H.P. Hratchian, A.F. Izmaylov, J. Bloino, G. Zheng, J.L. Sonnenberg, M. Hada, M. Ehara, K. Toyota, R. Fukuda, J. Hasegawa, M. Ishida, T. Nakajima, Y. Honda, O. Kitao, H. Nakai, T. Vreven, J.A. Montgomery Jr., J.E. Peralta, F. Ogliaro, M. Bearpark, J.J. Heyd, E. Brothers, K.N. Kudin, V.N. Staroverov, R. Kobayashi, J. Normand, K. Raghavachari, A. Rendell, J.C. Burant, S.S. Iyengar, J. Tomasi, M. Cossi, N. Rega, J.M. Millam, M. Klene, J.E. Knox, J.B. Cross, V. Bakken, C. Adamo, J. Jaramillo, R. Gomperts, R.E. Stratmann, O. Yazyev, A.J. Austin, R. Cammi, C. Pomelli, J.W. Ochterski, R.L. Martin, K. Morokuma, V.G. Zakrzewski, G.A. Voth, P. Salvador, J.J. Dannenberg, S. Dapprich, A.D. Daniels, Ö. Farkas, J.B. Foresman, J.V. Ortiz, J. Cioslowski, D.J. Fox, Gaussion09 C.01, 2009.
[32] A.D. Becke, Density-functional exchange-energy approximation with correct asymptotic behavior, Phys. Rev. A 38 (6) (1988) 3098–3100.
[33] A.D. Becke, Density-functional thermochemistry. III. The role of exact exchange, J. Chem. Phys 98 (1993) 5648–5652.
[34] W. Kohn, L. Sham, Self-consistent equations including exchange and correlation effects, Phys. Rev. (140) (1965) A1133–A1138.

[35] C. Lee, W. Yang, R.G. Parr, Development of the Colle-Salvetti correlation-energy formula into a functional of the electron density, Phys. Rev. B 37 (2) (1988) 785–789.
[36] T. Dunning, P.J. Hay, Gaussian basis sets for molecular calculations, in: Methods of Electronic Structure Theory, Springer, 1977, pp. 1–28.
[37] R. Dennington, T. Keith, J. Millam, GaussView 5.0.9, 2009.
[38] T. Yanai, D.P. Tew, N.C. Handy, A new hybrid exchange–correlation functional using the Coulomb-attenuating method (CAM-B3LYP), Chem. Phys. Lett. 393 (1-3) (2004) 51–57.
[39] J. Tomasi, B. Mennucci, E. Cances, The IEF version of the PCM solvation method: an overview of a new method addressed to study molecular solutes at the QM ab initio level, J. Mol. Struct. THEOCHEM 464 (1-3) (1999) 211–226.
[40] S.I. Büyükekşi, M. Durmuş, D. Atilla, Photophysical and photochemical properties of novel peripherally triethyleneoxysulfanyl substituted monomeric and Si–Si bonded dimeric silicon phthalocyanines, J. Porphyrins Phthalocyanines 20 (2016) 1426–1437.
[41] Z. Odabaş, H. Kara, A.R. Özkaya, M. Bulut, Synthesis, characterization and electrochemical properties of novel β 7-oxy-4-(4-methoxyphenyl)-8-methylcoumarin substituted metal-free, Zn (II) and Co (II) phthalocyanines, Polyhedron 39 (1) (2012) 38–47.
[42] A. Giraudeau, A. Louati, M. Gross, J. Andre, J. Simon, C. Su, K. Kadish, Redox properties of octacyano-substituted zinc phthalocyanine ((CN) 8PcZn). New charge-transfer complex, J. Am. Chem. Soc. 105 (9) (1983) 2917–2919.
[43] J. Wang, Analytical Electrochemistry, 2nd Ed., 2000.
[44] M. Sheik-Bahae, A.A. Said, T.-H. Wei, D.J. Hagan, E.W. Van Stryland, Sensitive measurement of optical nonlinearities using a single beam, IEEE J. Quantum Electron. 26 (4) (1990) 760–769.
[45] S.M. O'Flaherty, J.J. Doyle, W.J. Blau, Numerical approach for optically limited pulse transmission in polymer-phthalocyanine composite systems, J. Phys. Chem. B 108 (45) (2004) 17313–17319.
[46] S. Tekin, U. Kürüm, M. Durmuş, H.G. Yaglioglu, T. Nyokong, A. Elmali, Optical limiting properties of zinc phthalocyanines in solution and solid PMMA composite films, Opt. Commun. 283 (23) (2010) 4749–4753.
[47] J.J. Doyle, J. Wang, S.M. O'Flaherty, Y. Chen, A. Slodek, T. Hegarty, L.E. Carpenter, D. Wöhrle, M. Hanack, W.J. Blau, Nonlinear optical performance of chemically tailored phthalocyanine–polymer films as solid-state optical limiting devices, J. Opt. A 10 (7) (2008) 075101.
[48] Y. Liu, Y. Chen, L. Cai, J. Wang, Y. Lin, J. Doyle, W. Blau, Optical limiting properties of axially substituted indium phthalocyanines in the solid PMMA composite films, Mater. Chem. Phys. 107 (2-3) (2008) 189–192.
[49] M.A. Özdağ, T. Ceyhan, H. Ünver, A. Elmali, Ö. Bekaroğlu, Strong optical limiting property of a ball-type supramolecular zinc-phthalocyanine in polymer-phthalocyanine composite film, Opt. Commun. 283 (2) (2010) 330–334.
[50] J. Savolainen, D. van der Linden, N. Dijkhuizen, J.L. Herek, Characterizing the functional dynamics of zinc phthalocyanine from femtoseconds to nanoseconds, J. Photochem. Photobiol. A 196 (1) (2008) 99–105.